Mon. Not. R. Astron. Soc. **397,** 1915–1925 (2009) doi:10.1111/j.1365-2966.2009.14877.x

The nature of the young and low-mass open clusters Pismis 5, vdB 80, NGC 1931 and BDSB 96

C. Bonatto⋆ and E. Bica⋆

Departamento de Astronomia, Universidade Federal do Rio Grande do Sul Av. Bento Gonçalves 9500, Porto Alegre 91501-970, RS, Brazil

Accepted 2009 April 6. Received 2009 April 3; in original form 2009 March 5

ABSTRACT

We investigate the nature of four young and low-mass open clusters (OCs) located in the second and third quadrants with near-infrared Two-Micron All Sky Survey (2MASS) photometry (errors <0.1 mag). After field decontamination, the colour–magnitude diagrams (CMDs) display similar morphologies: a poorly populated main sequence (MS) and a dominant fraction of pre-MS (PMS) stars somewhat affected by differential reddening. Pismis 5, vdB 80 and BDSB 96 have MS ages within 5 ± 4 Myr, while the MS of NGC 1931 is 10 ± 3 Myr old. However, non-instantaneous star formation is implied by the wider ($\sim$20 Myr) PMS age spread. The cluster masses derived from MS+PMS stars are low, within $\sim$60–180 $M_{\odot}$, with mass functions (MFs) significantly flatter than Salpeter's initial mass function (IMF). Distances from the Sun are within 1.0–2.4 kpc, and the visual absorptions are in the range $A_V = 1.0$–2.0. From the stellar radial density profiles (RDPs), we find that they are small ($R_c \lesssim 0.48$ pc, $R_{RDP} \lesssim 5.8$ pc), especially Pismis 5 with $R_c \approx 0.2$ pc and $R_{RDP} \approx 1.8$ pc. Except for the irregular and cuspy inner regions of NGC 1931 and Pismis 5, the stellar RDPs follow a King-like profile. At $\sim$10 Myr, central cusps – which in old clusters appear to be related to advanced dynamical evolution – are probably associated with a star formation and/or molecular cloud fragmentation effect. Despite the flat MFs, vdB 80 and BDSB 96 appear to be typical young, low-mass OCs. NGC 1931 and especially Pismis 5, with irregular RDPs, low cluster mass and flat MFs, do not appear to be in dynamical equilibrium. Both may be evolving into OB associations and/or doomed to dissolution in a few 10^7 yr.

Key words: open clusters and associations: general – open clusters and associations: individual: Pismis 5 – open clusters and associations: individual: vdB 80 – open clusters and associations: individual: NGC 1931 – open clusters and associations: individual: BDSB 96.

1 INTRODUCTION

The first few 10 Myr represent the most critical phase in the life of a star cluster, to the point that only about 5 per cent (e.g. Lada & Lada 2003) of the embedded clusters are able to dynamically evolve into bound open clusters (OCs). The rapid gas removal by supernovae and massive star winds associated with this period can produce important changes on the primordial gravitational potential. Obviously, this effect depends essentially on the star-formation efficiency, the actual mass of primordial gas converted into stars and the mass of the more massive stars.

Because of the rather rapidly reduced potential, a significant fraction of the stars – the low mass ones in particular – moving faster than the scaled-down escape velocity may be driven into the field. Over a time-scale of 10–40 Myr, this process in turn, can dissolve most of the very young star clusters (e.g. Goodwin & Bastian 2006).

Observationally, low-mass star clusters younger than about 10 Myr present an underpopulated, developing main sequence (MS) and a more conspicuous population of pre-MS (PMS) stars. Typical examples are NGC 6611 (Bonatto, Santos & Bica 2006), NGC 4755 (Bonatto et al. 2006b), NGC 2239 and NGC 2244 (Bonatto & Bica 2009b) and Bochum 1 (Bica, Bonatto & Dutra 2008a). On a large scale, the important changes to the potential that affect the early cluster spatial structure should also be reflected on the stellar radial density profile (RDP). Bochum 1 and NGC 2244, for instance, can be taken as representative of this scenario, in which an irregular RDP cannot be represented by a cluster-like (i.e. an approximately isothermal sphere) profile. Such conspicuous RDP irregularities suggest significant profile erosion or dispersion of stars from a primordial cluster (e.g. Bica et al. 2008; Bonatto & Bica 2009b).

⋆E-mail: charles@if.ufrgs.br (CB); bica@if.ufrgs.br (EB)

In some cases, early star cluster dissolution may lead to the formation of low-mass OB associations, the subsequent dispersion of which may be an important source of field stars (e.g. Massey, Johnson & Gioia-Eastwood 1995). Bochum 1, with an irregular and clumpy RDP, can be an example of such an evolving structure. In this context, NGC 2244 appears to be another example of a young OC in the process of dissolving in a few 10^7 yr. Perhaps the difference between objects like Bochum 1 and NGC 2244 and *normal* young OCs (i.e. with the combined population of MS and PMS stars distributed according to a cluster RDP as in NGC 6611 and NGC 4755) is related to the interplay between environment conditions, star-formation efficiency and stellar mass. Interestingly, the mass stored in the MS+PMS members of Bochum 1 and NGC 2244 is a factor of 2–3 lower than those of NGC 6611 and NGC 4755.

In this paper, we investigate the nature of the poorly studied, young and low-mass OCs Pismis 5, vdB 80, NGC 1931 and BDSB 96, by means of their photometric and structural properties. Their location in the Galaxy, in the second and third quadrants (Table 1), minimizes field-star contamination (e.g. Bica, Bonatto & Camargo 2008b; Bonatto & Bica 2008b), which is essential when PMS stars are expected to dominate in colour–magnitude diagrams (CMDs). Our main goal is to determine whether such young and low-mass systems can be characterized as typical OCs or if they are on their way to dissolution. In addition, we will derive their fundamental and structural parameters, most of these for the first time.

This paper is organised as follows. In Section 2, we recall literature data on the target objects, discuss the Two Micron All Sky Survey (2MASS) photometry and build the field-star decontaminated CMDs. In Section 3, we derive fundamental cluster parameters. In Section 4, we derive structural parameters. In Section 5, we estimate cluster mass. In Section 6, we compare structural parameters and dynamical state with those of a sample of nearby OCs. Concluding remarks are given in Section 7.

2 THE OCS AND THE 2MASS PHOTOMETRY

The optical environments of the objects are shown in $10 \times 10\,\mathrm{arcmin}^2$ Digital Sky Survey (DSS)[1] B images (Fig. 1), in which nebular gas and/or dust emission is present in varying proportions. The embedded clusters show up in the $4 \times 4\,\mathrm{arcmin}^2$ 2MASS K_s images (Fig. 2).

Pismis 5 (also known as ESO 313−SC7) is located in Vela and its field contains a few relatively bright stars mixed with gas emission and dust (Fig. 1, top-left panel). It was discovered by P. Pismis (Pismis 1959) on Schmidt plates from the Tonantzintla Observatory (Mexico). According to SIMBAD,[2] the two brightest stars in this field are $CD-39\,4582$ [$\alpha(2000) = 08^h37^m38\overset{s}{.}0$, $\delta(2000) = -39°35'02''$, $V = 9.9$, $J = 9.4$, $K_s = 9.1$] and $CD-39\,4599$ [$\alpha(2000) = 08^h38^m1\overset{s}{.}8$, $\delta(2000) = -39°34'6\overset{''}{.}1$, $V = 10.0$, $J = 10.0$, $K_s = 9.9$]. Both appear to be members of Pismis 5 (Fig. 5). As far as we are aware, the only work on Pismis 5 is the UBV+ H_β photometric survey by Vogt & Moffat (1973), in which it was not considered as a star cluster.

Cradled inside the reflection nebula vdB-RN 80 (van den Bergh 1966) in Monoceros, the field of the star cluster vdB 80 (Fig. 1, top-right panel) is similar to that of Pismis 5. The brightest star *NSV* 2998 [SIMBAD: $\alpha(2000) = 06^h30^m49\overset{s}{.}8$,

[1] Extracted from the Canadian Astronomy Data Centre (CADC) – http://cadcwww.dao.nrc.ca/.
[2] http://simbad.u-starsbg.fr/simbad

Table 1. Fundamental parameters of the target OCs

	Literature						This work								
Cluster	$\alpha(2000)$	$\delta(2000)$	Age	$E(B-V)$	$d_\odot$	D	Source	$\alpha(2000)$	$\delta(2000)$	ℓ	b	Age	$E(B-V)$	$d_\odot$	ΔR_{SC}	R_{ext}
	(h m s)	(° ′ ″)	(Myr)	(mag)	(kpc)	(arcmin)		(h m s)	(° ′ ″)	(°)	(°)	(Myr)	(mag)	(kpc)	(kpc)	(′)
(1)	(2)	(3)	(4)	(5)	(6)	(7)	(8)	(9)	(10)	(11)	(12)	(13)	(14)	(15)	(16)	(17)
Pismis 5	08:37:38	−39:35:00	15	0.42	0.87	5.0	1	08:37:37.5	−39:34:10.5	259.33	+0.93	5 ± 4	0.42 ± 0.03	1.0 ± 0.1	+0.3 ± 0.1	40
vdB 80	06:30:48	−09:40:00	4.5	0.38	–	5.0	1	06:30:50.2	−09:39:18.0	219.26	−8.93	5 ± 2	0.61 ± 0.10	2.1 ± 0.3	+1.7 ± 0.3	40
NGC 1931	05:31:25	+34:14:32	10	0.74	3.1	4.0	1	05:31:24.7	+34:14:41.2	173.90	+0.28	10 ± 3	0.62 ± 0.10	2.4 ± 0.3	+2.4 ± 0.4	60
BDSB 96	07:05:18	−12:19:44	–	–	1.1	2.7	2	07:05:17.3	−12:19:9.5	225.46	−2.57	5 ± 3	0.37 ± 0.10	1.4 ± 0.2	+1.0 ± 0.2	60

Notes. Sources: (1) – WEBDA[13]; (2) – Bica et al. (2003). Column 7: optical diameter; Column 15: distance from the Sun; Column 16: distance from the solar circle; Column 17: extraction radius.

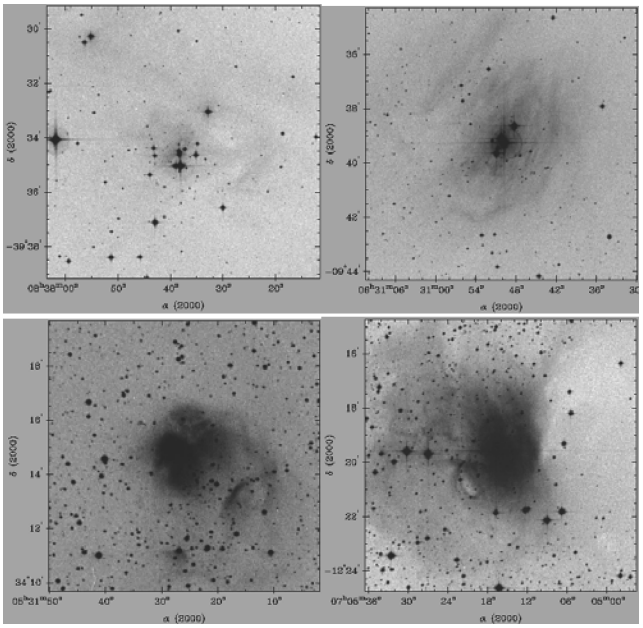

Figure 1. The optical environments are shown in 10×10 arcmin^2 DSS B images of Pismis 5 (top-left panel), vdB 80 (right-hand panel), NGC 1931 (bottom-left panel) and BDSB 96 (right-hand panel). Gas emission, dust reflection and/or absorption are present in all fields in varying proportions. Orientation: north to the top and east to the left.

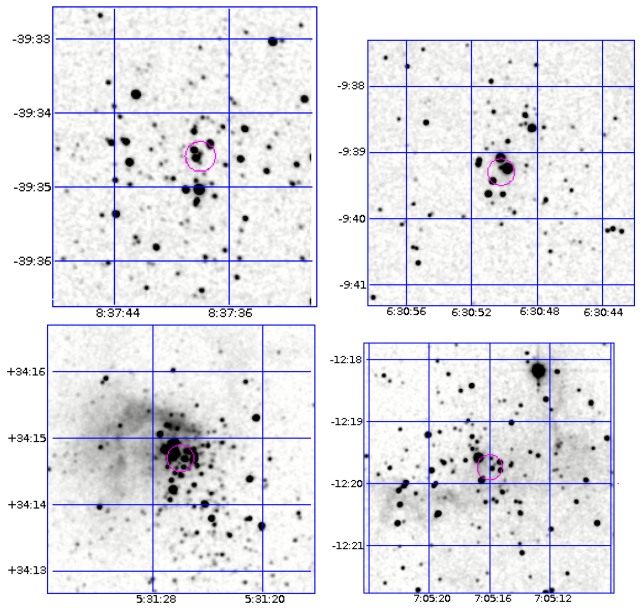

Figure 2. 4×4 arcmin^2 2MASS K_s images showing the embedded clusters Pismis 5 (top-left panel), vdB 80 (right-hand panel), NGC 1931 (bottom-left panel) and BDSB 96 (right-hand panel). Right ascension and declination are given in the abscissa and ordinate, respectively. Orientation: north to the top and east to the left.

$\delta(2000) = -09^\circ 39' 14\farcs8$, $V = 8.8$, $J = 8.1$, $K_s = 8.1$] appears to be the only MS member of vdB 80 (Fig. 5). In the only reference to vdB 80 as a star cluster, Ahumada et al. (2001) estimated the age 4.5 ± 1.5 Myr by means of integrated spectra.

The star cluster NGC 1931 (Stock 9, Collinder 68) lies within the bright nebula NGC 1931 (Sh 2-237) in Auriga. Moffat, Fitzgerald & Jackson (1979) determined the distance from the Sun $d_\odot = 1.8$ kpc, while Pandey & Mahra (1986) found $d_\odot = 2.2$ kpc. Bhatt et al. (1994) found $d_\odot = 2.2$ kpc, $E(B-V) = 0.55$ and the age ∼10 Myr. Lata et al. (2002) derived $E(B-V) = 0.58$ and ∼13 Myr. Finally, Chen, Chen & Shu (2004) found $d_\odot = 3.1$ kpc, ∼10 Myr and the cluster radius $R = 4.13$ arcmin. The latter work was based on 2MASS photometry, as in the present study with our tools, since the cluster is embedded in nebular emission.

Discovered in a survey of infrared embedded star clusters and stellar groups carried with 2MASS by Bica et al. (2003), BDSB 96 (in the nebula Cederblad 90, also known as Gum 3, Sh 2-297, RCW 1a, vdB-RN 94 and Ber 134) in Canis Major, was classified as an infrared OC located at about 1.1 kpc from the Sun. Its field contains the single bright star *HD* 53623 [SIMBAD: $\alpha(2000) = 07^h05^m16\fs7$, $\delta(2000) = -12^\circ 19' 34\farcs5$, $V = 8.0$, $J = 8.0$, $K_s = 8.0$], which is in the MS of BDSB 96 (Fig. 6). Nebular gas and/or dust emission is more conspicuous in its field (Fig. 1, bottom-right panel) than in Pismis 5, vdB 80 and NGC 1931.

Table 1 provides parameters found in the literature and derived here. Since accurate spectral types of the bright stars listed above are not available, spectroscopic distances cannot be computed. The central coordinates were recomputed to match the absolute maximum present in the stellar surface densities (Section 2.3).

2.1 2MASS photometry

The present OCs still retain part of the primordial gas and dust (Fig. 1), which makes the near-infrared the optimal spectral range to probe them. For instance, the number of detected stars at a given radius in NGC 2244 in the optical is significantly lower than in the near-infrared, dropping to about 5 per cent for the full field (Bonatto & Bica 2009b). For this purpose, we work with the 2MASS[3] near-infrared J, H and K_s photometry, which allows the spatial and photometric uniformity useful for wide extractions that, in turn, provide high star-count statistics. Within this perspective, we have been developing quantitative tools to statistically disentangle cluster evolutionary sequences from field stars in CMDs. Decontaminated CMDs, in turn, have been used to investigate the nature of cluster candidates and derive their astrophysical parameters (e.g. Bica et al. 2008b). In short, we apply (i) field-star decontamination to uncover the intrinsic CMD morphology, essential for a proper derivation of reddening, age and distance from the Sun, and (ii) colour–magnitude filters, which are essential for intrinsic stellar RDPs, as well as luminosity and mass functions (MFs). In particular, the use of field-star decontamination in the construction of CMDs has proved to constrain age and distance more than working with raw (observed) photometry, especially for low-latitude OCs (Bonatto et al. 2006a).

2MASS can reach adequate CMD depths for nearby OCs. For instance, our group has studied the young OCs NGC 6611, NGC 4755, NGC 2239 and NGC 2244. Abundant PMS stars were seen in the ≈1 Myr old NGC 6611 (which is essentially embedded) and the 1–6 Myr old NGC 2244, and a few remaining ones in the ≈14 Myr old NGC 4755. As nearby older OCs we cite NGC 2477 (Bonatto & Bica 2005) and M 67 (Bonatto & Bica 2003).

Photometry was extracted in a wide circular field of radius R_{ext} (Table 1) with VizieR.[4] The extraction radii are large enough to allow determination of the background level (Section 4) and

[3] The 2MASS, All Sky data release (Skrutskie et al. 1997) – http://www.ipac.caltech.edu/2mass/releases/allsky/.
[4] http://vizier.u-strasbg.fr/viz-bin/VizieR?-source=II/246

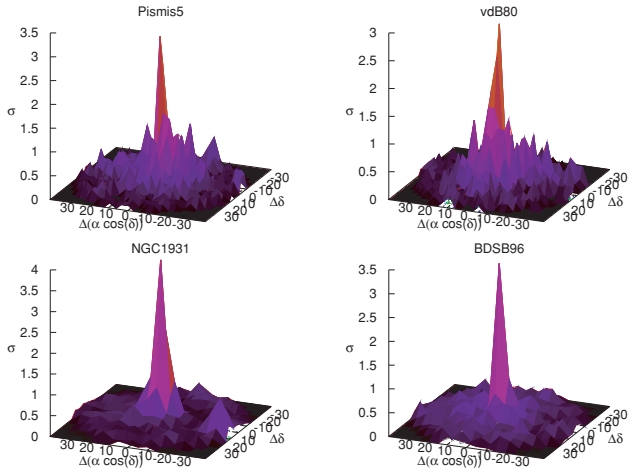

Figure 3. Stellar surface-density σ(stars arcmin^{-2}) computed with field-decontaminated photometry to enhance the cluster/background contrast. $\Delta[\alpha\ \cos\ (\delta)]$ and $\Delta\delta$ in arcmin.

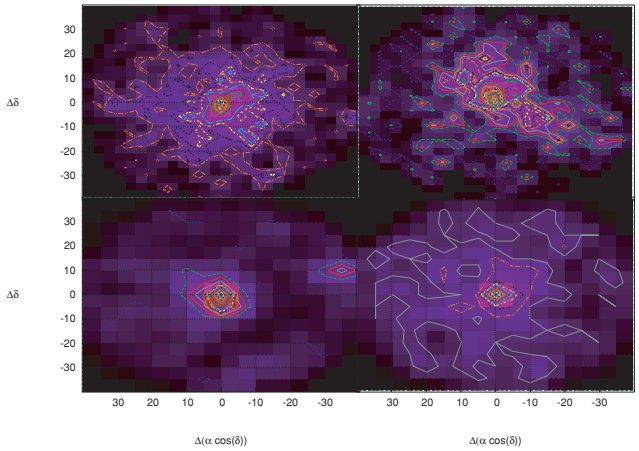

Figure 4. Similar to Fig. 3 for the isopleth curves, for a better visualization of cluster extent and geometry.

to statistically characterize the colour and magnitude distribution of the field stars (Section 2.2). As photometric quality constraint, only stars with J, H and K_s errors lower than 0.1 mag were considered.[5] Reddening corrections are based on the relations $A_J/A_V = 0.276$, $A_H/A_V = 0.176$, $A_{K_S}/A_V = 0.118$ and $A_J = 2.76 \times E(J-H)$ given by Dutra, Santiago & Bica (2002), with $R_V = 3.1$, considering the extinction curve of Cardelli, Clayton & Mathis (1989).

2.2 Field decontamination

Field-star decontamination is a very important step in the identification and characterization of star clusters, especially the clusters near the Galactic equator. Different approaches are described in Bonatto & Bica (2009b). In this paper, we employ the decontamination algorithm detailed in Bonatto & Bica (2007a), Bica et al. (2008b) and Bica & Bonatto (2008), and briefly described below.

The algorithm (i) divides the whole range of CMD magnitude and colours into a 3D grid of cells with axes along the J magnitude and the $(J-H)$ and $(J-K_s)$ colours, (ii) estimates the number density of field stars in each cell based on the number of comparison field stars with similar magnitude and colours as those in the cell and (iii) subtracts the estimated number of field stars from each cell. Typical cell dimensions are $\Delta J = 1.0$ and $\Delta(J-H) = \Delta(J-K_s) = 0.2$; the comparison fields are located within $R = 30$ arcmin and the extraction radius. With this setup, the subtraction efficiency, that is the difference between the background contamination (which may be fractional) and the number of subtracted stars in each cell (e.g. Bonatto & Bica 2008b), summed over all cells, is higher than 90 per cent in all cases.

2.3 Decontaminated surface density maps

Fig. 3 shows the spatial distribution of the stellar surface-density (σ, in units of stars arcmin^{-2}) around the four objects, measured with 2MASS photometry. We use field-star decontaminated photometry (Section 2.2) to maximize the cluster/background contrast. The surface density is computed in a rectangular mesh with cells 2.5×2.5 arcmin^2 wide, reaching total offsets of $|\Delta[\alpha\ \cos\ (\delta)]| = |\Delta\delta| \approx 40$ arcmin with respect to the cluster centre (Table 1). Despite the gas and dust associated with the present low-mass clusters (Fig. 1), the central excesses are conspicuously detected in the decontaminated surface-density distributions. Besides, the residual surface-density around the centre has been reduced to a minimum level.

By design, our decontamination depends essentially on the colour–magnitude distribution of stars located in different spatial regions. The fact that the decontaminated surface-density presents a conspicuous excess only at the assumed cluster position implies significant differences between this region and the comparison field, both in terms of colour–magnitude and star counts within the corresponding colour–magnitude bins. This meets cluster expectations, which can be characterized by a single-stellar population, projected against a Galactic stellar field.

The respective isopleth surface maps are shown in Fig. 4, in which cluster size and geometry can be observed. In all cases, the central region ($R < 5$ arcmin) appears essentially circular, with elongated external regions, especially NGC 1931.

3 FUNDAMENTAL PARAMETERS

$J \times (J-K_s)$ CMDs built with the raw photometry of the sample objects are shown in the top panels of Figs 5 and 6. In all cases, the sampled region contains most of the cluster stars (Fig. 10). When qualitatively compared with the CMDs extracted from the equal-area comparison field[6] (middle panels), features typical of very young OCs emerge: a relatively vertical and poorly populated MS together with a large number of faint and red PMS stars.

The decontaminated CMDs are shown in the bottom panels of Figs 5 and 6. As expected, essentially all contamination is removed, leaving stellar sequences typical of mildly reddened, young and low-mass OCs, with a developing MS and a significant population of PMS stars.

[5] In all cases, the bright stars have photometric errors within the adopted range. Besides, any bias against low-mass stars (larger errors) introduced by this criterion (applied equally for cluster and field stars) is probably minimized by the field decontamination (Section 2.2).

[6] The equal-area field extractions serve only for qualitative comparisons, since the decontamination uses a large surrounding area (Section 2.2).

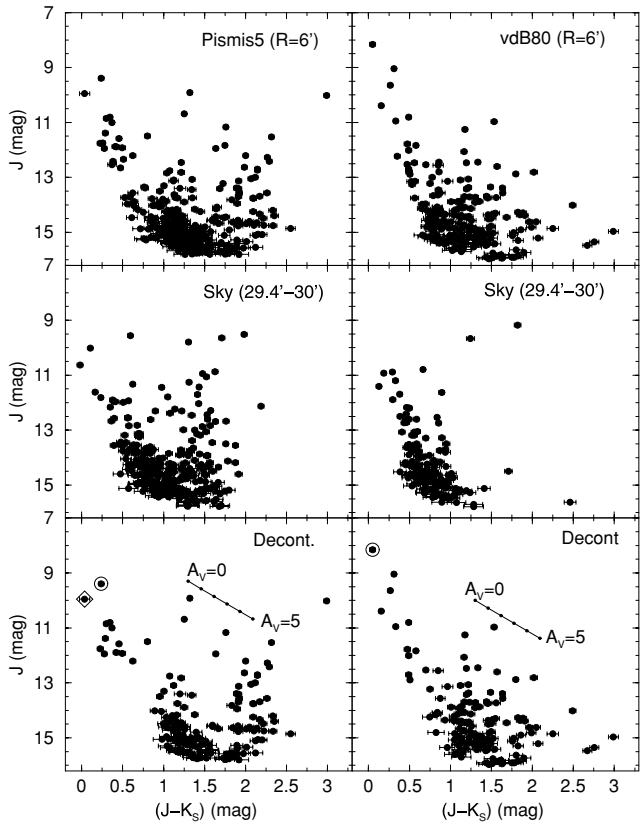

Figure 5. 2MASS CMDs of Pismis 5 (left-hand panel) and vdB 80 (right-hand panel). Top panels: observed photometry. Middle: equal-area comparison field CMDs. Bottom: decontaminated CMDs. Bright stars in common with SIMBAD are: $CD-39\,4582$ (large circle) and $CD-39\,4599$ (diamond) in Pismis 5, and NSV 2998 (large circle) in vdB 80. Reddening vectors for $A_V = 0$–5 are shown in the bottom panels.

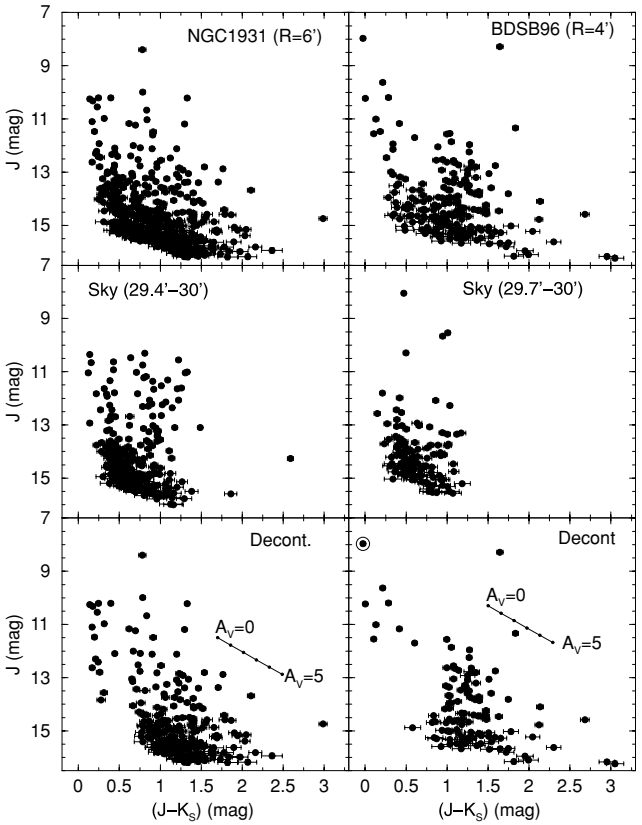

Figure 6. Similar to Fig. 5 for NGC 1931 (left-hand panel) and BDSB 96 (right-hand panel). The bright star in BDSB 96 is HD 53623.

Colour distributions wider than the spread predicted by PMS models occur in all cases (Fig. 7), which reflects differential reddening. To examine this issue, we show in Figs 5–7 reddening vectors computed with the 2MASS ratios (Section 2.1) for visual absorptions $A_V = 0$–5. Taking into account the PMS isochrone fit (Fig. 7), the differential reddening appears to be lower than $A_V = 5$.

We base the fundamental parameter derivation on the field-decontaminated CMD morphologies (Fig. 7), using as constraint the combined MS and PMS star distribution. We adopt solar metallicity isochrones because the clusters are young and located not far from the solar circle (see below), a region essentially occupied by [Fe/H] ≈ 0.0 OCs (Friel 1995).

To represent the MS, we use Padova isochrones (Girardi et al. 2002) computed with the 2MASS J, H and K_s filters.[7] The similar decontaminated CMD morphologies, typical of young ages (Fig. 7), indicate similar age-solutions for the present objects.

Sophisticated CMD fit approaches are available, especially for the MS (as summarized in Naylor & Jeffries 2006). However, given the poorly populated MSs, the 2MASS photometric uncertainties for the lower sequences and the important population of PMS stars, we decided for the direct comparison of isochrones with the decontaminated CMD morphology. Thus, fits are made *by eye*, taking the combined MS and PMS stellar distributions as constraint, allowing as well for differential reddening and photometric uncertainties. Isochrones of Siess, Dufour & Forestini (2000) with ages in the range 0.2–20 Myr are used to characterize the PMS sequences. The results are shown in Fig. 7 and discussed below.

Pismis 5: given the poorly populated MS, acceptable fits to the decontaminated MS morphology are obtained with any isochrone with age in the range 1–10 Myr. The PMS stars are basically contained within the 0.2 and 10 Myr isochrones as well, which implies a similar age range as the MS. Thus, we take the 5 Myr isochrone as representative solution, with a 4 Myr spread. In this case, $CD-39\,4599$ is in the MS while $CD-39\,4582$ would be a massive ($\sim$5 $M_\odot$) PMS almost reaching the MS.

With the adopted solution, the fundamental parameters of Pismis 5 are the near-infrared reddening $E(J-H) = 0.13 \pm 0.01$ [$E(B-V) = 0.42 \pm 0.03$ or $A_V = 1.3 \pm 0.1$], the observed and absolute distance moduli $(m-M)_J = 10.4 \pm 0.1$ and $(m-M)_O = 10.04 \pm 0.10$, respectively, and the distance from the Sun $d_\odot = 1.0 \pm 0.1$ kpc. We adopt $R_\odot = 7.2 \pm 0.3$ kpc (Bica et al. 2006) as the Sun's distance to the Galactic Centre to compute Galactocentric distances.[8] For $R_\odot = 7.2$ kpc, the Galactocentric distance of

[7] http://stev.oapd.inaf.it/cgi-bin/cmd. These isochrones are very similar to the Johnson–Kron–Cousins ones (e.g. Bessel & Brett 1988), with differences of at most 0.01 in colour (Bonatto, Bica & Girardi 2004).

[8] Derived by means of the Globular Cluster (GC) spatial distribution. Recently, Trippe et al. (2008) found $R_{GC} = 8.07 \pm 0.32$ kpc while Ghez et al. (2008) found $R_{GC} = 8.0 \pm 0.6$ kpc or $R_{GC} = 8.4 \pm 0.4$ kpc, under different assumptions.

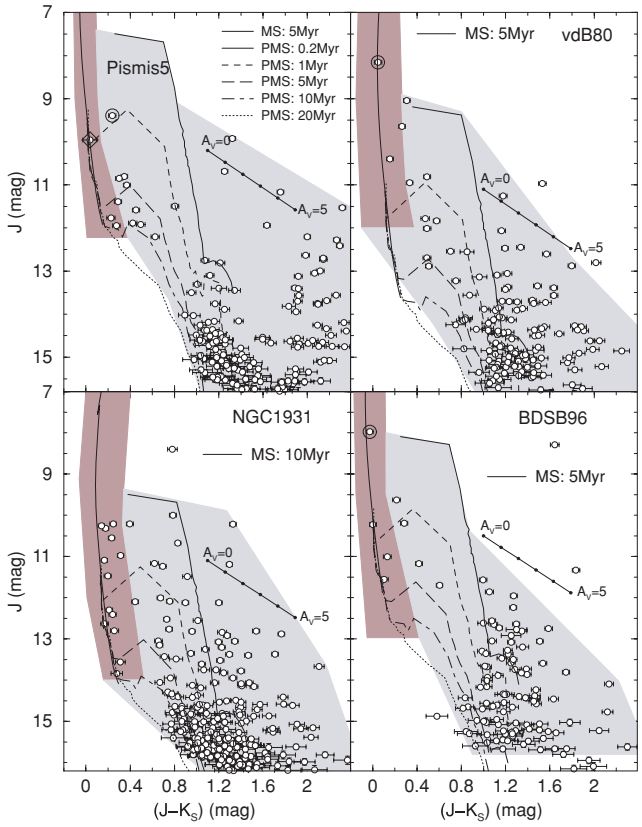

Figure 7. Adopted MS+PMS isochrone solutions to the decontaminated CMDs. SIMBAD bright stars and reddening vectors as in Figs 5 and 6. Shaded polygons show the MS (dark grey) and PMS (light grey) colour–magnitude filters (Section 4).

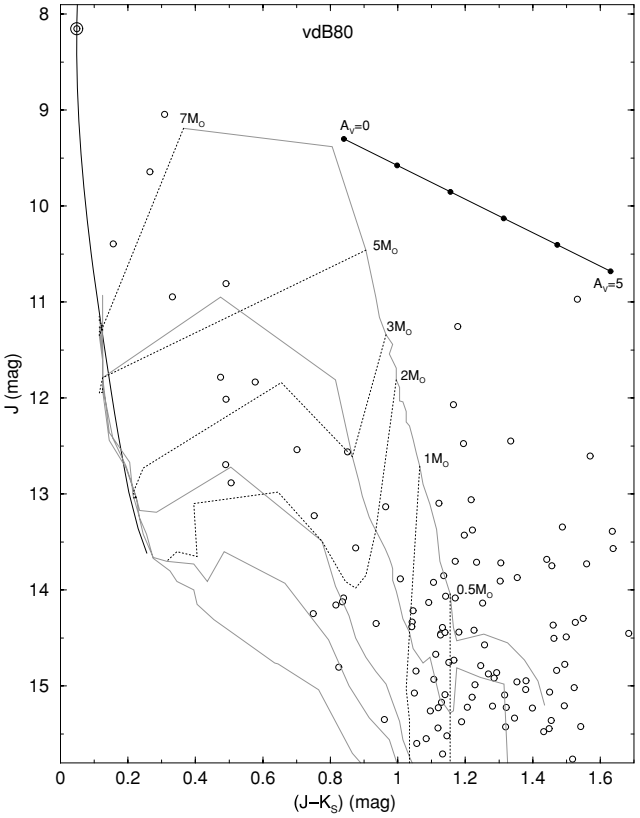

Figure 8. Decontaminated CMD of vdB 80, used to illustrate the PMS mass estimate. Light lines: MS and PMS isochrones set as in Fig. 7. Heavy dotted: PMS evolutionary tracks for different masses.

Pismis 5 is $R_{GC} = 7.5 \pm 0.1$ kpc, which puts it ≈0.3 kpc outside the solar circle. This solution is shown in Fig. 7.

vdB 80: the bright star *NSV* 2998 ($J = 8.153$) helps constrain the MS age to 5 ± 2 Myr, which agrees with the 4.5 ± 1.5 Myr age of Ahumada et al. (2001). Similarly to Pismis 5, the PMS stars are essentially found within the 0.2–10 Myr isochrones. With this solution, the fundamental parameters of vdB 80 are $E(J - H) = 0.19 \pm 0.03$ [$E(B - V) = 0.61 \pm 0.10$ or $A_V = 2.0 \pm 0.3$], $(m - M)_J = 12.1 \pm 0.3$, $(m - M)_O = 11.58 \pm 0.31$, $d_\odot = 2.1 \pm 0.3$ kpc, and $R_{GC} = 8.9 \pm 0.3$ kpc, thus ≈1.7 kpc outside the solar circle.

NGC 1931: besides the most populated MS of the present sample, NGC 1931 presents the smallest gap between the faintest MS star and the PMS distribution, which suggest a more evolved phase. Indeed, the PMS stars distribute between the 0.2–20 Myr isochrones. Based on this, the MS age can be set at 10 ± 3 Myr, which agrees with the estimates of Pandey & Mahra (1986), Bhatt et al. (1994), Lata et al. (2002) and Chen et al. (2004). This solution implies $E(J - H) = 0.19 \pm 0.03$ [$E(B - V) = 0.61 \pm 0.10$ or $A_V = 2.0 \pm 0.3$], $(m - M)_J = 12.4 \pm 0.3$, $(m - M)_O = 11.86 \pm 0.22$, $d_\odot = 2.4 \pm 0.2$ kpc, and $R_{GC} = 9.6 \pm 0.2$ kpc, thus ≈2.4 kpc beyond the solar circle. Our value for $d_\odot$ is intermediate between the 1.8 kpc of Moffat et al. (1979) and 3.1 kpc of Chen et al. (2004), and agrees with the 2.2 kpc of Pandey & Mahra (1986) and Bhatt et al. (1994).

BDSB 96: the CMD of this object is similar to that of vdB 80 – including the presence of a bright star (*HD* 53623) in the MS, which suggests a similar solution, with the MS age 5 ± 3 Myr. This solution implies $E(J - H) = 0.12 \pm 0.03$ [$E(B - V) = 0.37 \pm 0.10$ or $A_V = 1.1 \pm 0.3$], $(m - M)_J = 11.0 \pm 0.2$, $(m - M)_O = 10.68 \pm 0.22$, $d_\odot = 1.4 \pm 0.2$ kpc, and $R_{GC} = 8.2 \pm 0.2$ kpc, thus ≈1.0 kpc outside the solar circle. Our value of $d_\odot$ agrees with the 1.1 kpc of Bica et al. (2003).

Besides the MS age, the present objects have in common a significant age spread implied by the PMS stars. This indicates a non-instantaneous star formation process, similar to what was found in our previous studies of NGC 4755, 6611 and 2244.

3.1 Colour–colour diagrams

When transposed to the near-infrared colour–colour diagram $(J - K_s) \times (H - K_s)$ (Fig. 9), the age and reddening solutions derived for the present objects consistently match their field-star decontaminated photometry. Since they include PMS stars, we use tracks of Siess et al. (2000) to characterize the age. MS stars lie on the blue side of the diagram. As expected from the CMDs, a significant fraction of the stars appears to be very reddened. Besides, since most stars have $(H - K_s)$ colours close to the isochrone, within the uncertainties, the fraction of stars still bearing circunstellar discs (with excess in H) appears to be low (Bonatto et al. 2006b and references therein).

4 CLUSTER STRUCTURE

We use the RDPs, defined as the projected stellar number density around the cluster centre (i.e. the maximum of the surface density maps – Section 2.3), to derive structural parameters. To minimize noise, we work with colour–magnitude filters (shown in Fig. 7) to

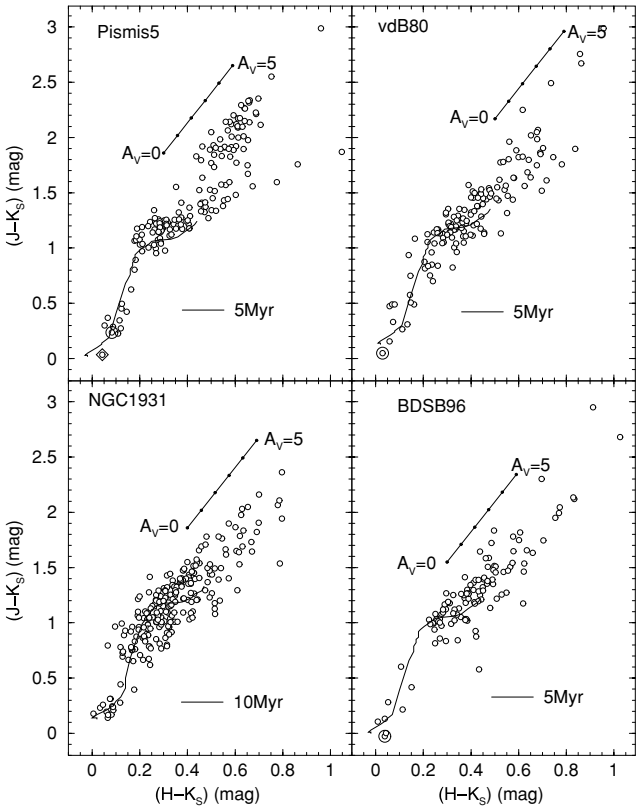

Figure 9. Decontaminated colour–colour diagrams. PMS isochrones set with the derived reddening values (Section 3). SIMBAD bright stars and reddening vectors as in Figs 5 and 6.

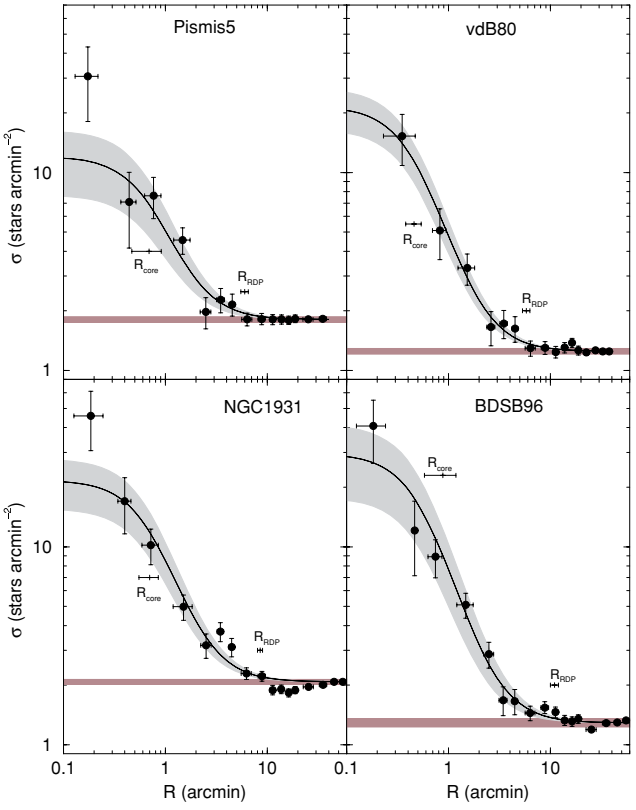

Figure 10. Stellar RDPs built with colour–magnitude filtered photometry together with the best-fitting King-like profile (solid line), the 1σ uncertainty (light-shaded region) and the background level (shaded polygon). Note the central cusp in the RDPs of Pismis 5 and NGC 1931.

exclude stars with colours unlike those of the cluster CMD morphology.[9] This enhances the RDP contrast relative to the background, especially in crowded fields (e.g. Bonatto & Bica 2007a). Examples of the advantage of using colour–magnitude filters can be found in, for example Bonatto & Bica (2007b), Bonatto, Bica & Santos (2008) and Bonatto & Bica (2008b).

Rings of increasing width with distance from the cluster centre are used to preserve spatial resolution near the centre and minimize noise at large radii. The set of ring widths used is $\Delta R = 0.25$, 0.5, 1.0, 2.0 and 5 arcmin, respectively, for $0 \leq R < 0.5$ arcmin, $0.5 \leq R < 2$ arcmin, $2 \leq R < 5$ arcmin, $5 \leq R < 20$ arcmin and $R \geq 20$ arcmin. Because of the low number of stars in the central parts of vdB 80, we used $\Delta R = 0.5$ for $R \leq 1$ arcmin. The residual background level of each RDP corresponds to the average number density of field stars. The R coordinate (and uncertainty) of each ring corresponds to the average position and standard deviation of the stars inside the ring. As a caveat, we note that the present OCs are not spherical, especially at the outskirts (Fig. 4), which might affect the RDPs for large radii. Because of this, deviations in the central parts of the RDP are not expected to be significant.

Minimization of the number of non-cluster stars by the colour–magnitude filters yielded RDPs (Fig. 10) highly contrasted relative to the background. For simplicity, we fit the RDPs with $\sigma(R) = \sigma_{\rm bg} + \sigma_0/[1 + (R/R_{\rm c})^2]$, where $\sigma_{\rm bg}$ is the residual background density, σ_0 is the central density of stars, and $R_{\rm c}$ is the core radius. This function, applied to star counts, is similar to that introduced by King (1962) to describe the surface-brightness profiles in the central parts of GCs.[10] To minimize degrees of freedom, σ_0 and $R_{\rm c}$ follow from the fit, while $\sigma_{\rm bg}$ is measured in the field and kept fixed. The best-fitting solutions and uncertainties are shown in Fig. 10, and the parameters in Table 2. We also estimate the cluster radius ($R_{\rm RDP}$), that is the distance from the centre where the cluster RDP and field fluctuations are statistically indistinguishable (e.g. Bonatto & Bica 2005), and the density contrast parameter $\delta_{\rm c} = 1 + \sigma_0/\sigma_{\rm bg}$ (Table 2). Interestingly, the density-contrast parameter reaches high values, $7 \lesssim \delta_{\rm c} \lesssim 23$, as expected from compact star clusters.

Within uncertainties, the adopted King-like function describes the RDPs of vdB 80 and BDSB 96 along the whole radius range. To a lesser degree, the same applies for Pismis 5 and NGC 1931, in which the innermost bin presents an excess over the fit. In old star clusters, such a cusp has been attributed to a post-core collapse structure, like those detected in some GCs (e.g. Trager, King & Djorgovski 1995). Gyr-old OCs, for example NGC 3960 (Bonatto & Bica 2006) and LK 10 (Bonatto & Bica 2009a), also display such feature, which is related to dynamical evolution. With respect to very young clusters, the RDPs of NGC 2244 (Bonatto & Bica 2009b) and NGC 6823 (Bica et al. 2008a) also present a central cusp, similarly to those in Pismis 5 and NGC 1931. Clusters are not expected to dynamically evolve into a post-core collapse on such short

[9] They are wide enough to include cluster MS and PMS stars, together with the photometric uncertainties and binaries (and other multiple systems).

[10] Besides, because of the relatively small number of stars in the present OCs, fluctuations in surface-brightness profiles are expected to be larger than those in RDPs. Alternative RDP fit functions are discussed in Bonatto & Bica (2008a).

Table 2. Derived structural parameters.

Cluster	σ_{bg} (* arcmin^{-2})	σ_0 (* arcmin^{-2})	R_c (arcmin)	R_{RDP} (arcmin)	δ_c	1 arcmin (pc)	σ_{bg} (* pc^{-2})	σ_0 (* pc^{-2})	R_c (pc)	R_{RDP} (pc)
(1)	(2)	(3)	(4)	(5)	(6)	(7)	(8)	(9)	(10)	(11)
Pismis 5	1.81 ± 0.02	10.2 ± 4.3	0.69 ± 0.22	6.0 ± 0.3	6.6 ± 2.3	0.296	20.7 ± 0.3	116.7 ± 49.2	0.20 ± 0.06	1.8 ± 0.1
vdB 80	1.25 ± 0.02	20.3 ± 5.0	0.46 ± 0.08	5.8 ± 0.3	17.2 ± 4.0	0.599	3.5 ± 0.1	56.4 ± 14.0	0.28 ± 0.05	3.5 ± 0.2
NGC 1931	2.08 ± 0.02	19.6 ± 6.1	0.70 ± 0.15	8.5 ± 0.5	10.4 ± 2.9	0.684	4.4 ± 0.1	41.9 ± 13.0	0.48 ± 0.10	5.8 ± 0.3
BDSB 96	1.29 ± 0.01	28.2 ± 11.8	0.88 ± 0.30	11.0 ± 1.0	22.9 ± 9.2	0.397	8.1 ± 0.1	178.8 ± 74.8	0.35 ± 0.12	4.4 ± 0.4

Notes. Core (R_c) and cluster (R_{RDP}) radii are given in angular and absolute units. Column 6: cluster/background density contrast parameter ($\delta_c = 1 + \sigma_0/\sigma_{bg}$). Column 7: arcmin to parsec scale.

time-scales. Consequently, the cusp in young clusters must be related to molecular cloud fragmentation and/or star-forming effects, and may suggest early deviation from dynamical equilibrium (Section 6).

Taken at face value, the core radii of the present objects [$0.2 \lesssim R_c(pc) \lesssim 0.5$] fall on the low-$R_c$ tail of the distribution derived for a sample of relatively nearby OCs by Piskunov et al. (2007).

5 MASS ESTIMATE

The most conspicuous CMD feature of the present OCs is the dominant presence of PMS stars, followed by the poorly populated MS (Fig. 7). Obviously, in each cluster, most of the mass is stored in the PMS stars. Because the decontamination algorithm actually excludes stars (in integer numbers), the decontaminated photometry should be used essentially to determine the CMD morphology or the colour–colour distribution (Section 3). However, when magnitude (or alternatively mass) bins are used to build the MFs, the bin-to-bin subtraction of the comparison field (normalized to the same projected area as the cluster) contribution is expected to produce fractional numbers, which should be incorporated into the MFs (e.g. Bonatto & Bica 2005). For this reason, we use the colour–magnitude filtered photometry (Fig. 7) to estimate the cluster mass.

The number of MS stars is derived by counting the stars within $R \leq R_{RDP}$ (in bins of $\Delta J = 1$ mag), and subtracting those in the field (normalized to the same area). The corresponding stellar mass in each magnitude bin is taken from the mass–luminosity relation derived from the isochrone fit (Section 3). Summing the values in each magnitude bin produces the total number (n_{MS}) and mass (m_{MS}) of MS stars. A similar strategy is applied to the PMS stars. We consider the evolutionary tracks for the PMS masses 0.5, 1, 2, 3, 5 and 7 $M_\odot$ (Fig. 8). The number of PMS stars between any two tracks is counted for $R \leq R_{RDP}$ and the field, taking into account the reddening vectors. The average mass between two evolutionary tracks is taken as the mass of a respective PMS star. All tracks summed result in the number (n_{PMS}) and mass (m_{PMS}) of PMS stars (Table 3).

As anticipated by the CMDs (Fig. 7), the MSs as a rule are poorly populated. Pismis 5, vdB 80 and BDSB 96 contain about four MS stars, while NGC 1931 hosts about 15 MS stars. Such low numbers reflect the young age and low-mass nature of these objects. Indeed, the mass of the present objects, as derived from their MS+PMS members, is within 60–180 $M_\odot$.[11] For comparison, Bochum 1, NGC 6823, 2244 and 2239 contain 128, 65, 26 and 26 MS stars, respectively, while their (MS+PMS) masses are 720, 1150, 625 and 301 $M_\odot$, respectively.

An estimate of the MS and PMS MFs can be made with the approach described above. In Fig. 11, we show the resulting MFs for the PMS and MS stars combined. Since the MSs are very-poorly populated (Table 3), it should be noted that these MFs correspond essentially to the PMS stars; the MSs contribute somewhat to the range $m \gtrsim 2\,M_\odot$. Besides, given the simplifying assumptions, the error bars in the MFs are only formal, and should be taken as a lower limit. Bearing this in mind, the MFs can be represented by the function $\phi(m) = (dN/dm) \propto m^{-(1+\chi)}$, with slopes χ (Table 3) significantly flatter than the $\chi = 1.35$ of Salpeter (1955) initial mass function (IMF). Interestingly, these MFs do not appear to present a

[11] As a caveat, we note that because of the differential reddening and the 2MASS photometric limit, we may not detect the PMS stars of very-low mass; thus the mass values may be somewhat higher.

Table 3. MS and PMS stellar content.

		MS		PMS		MS+PMS		
Cluster	Δm ($M_\odot$)	n_{MS} (stars)	m_{MS} ($M_\odot$)	n_{PMS} (stars)	m_{PMS} ($M_\odot$)	n_{MS+PMS} (stars)	m_{MS+PMS} ($M_\odot$)	χ
(1)	(2)	(3)	(4)	(5)	(6)	(7)	(8)	(9)
Pismis 5	1.9-13.4	3 ± 1	12 ± 3	100 ± 20	46 ± 7	103 ± 21	58 ± 8	-0.03 ± 0.19
vdB 80	2.3-21.6	4 ± 1	40 ± 11	108 ± 12	55 ± 13	112 ± 13	95 ± 17	-0.24 ± 0.09
NGC 1931	2.0-17.8	15 ± 3	62 ± 13	183 ± 33	115 ± 37	198 ± 34	177 ± 39	-0.02 ± 0.08
BDSB 96	1.8-23.8	5 ± 1	23 ± 6	171 ± 23	131 ± 21	176 ± 24	154 ± 23	$+0.80 \pm 0.08$

Notes. Column 2: Effective MS mass range. Column 9: MS+PMS MF slope χ, derived from the fit of $\phi(m) \propto m^{-(1+\chi)}$.

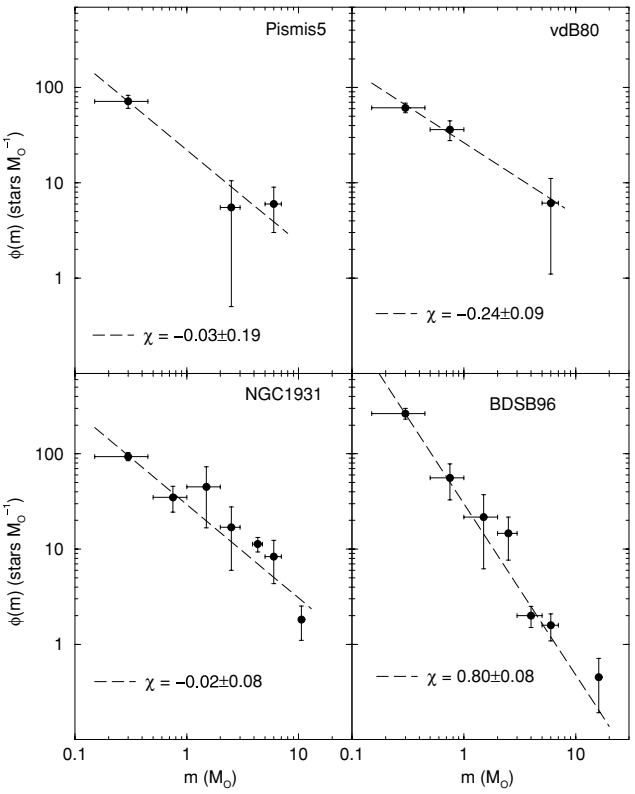

Figure 11. MS+PMS MFs fitted by the function $\phi(m) \propto m^{-(1+\chi)}$ (dashed line).

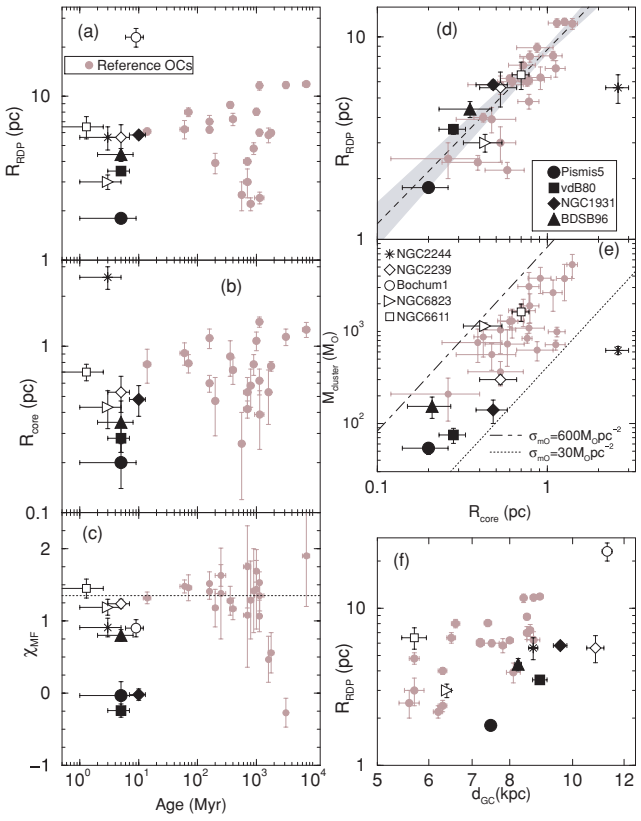

Figure 12. Diagrams dealing with astrophysical parameters of OCs. Grey-shaded circles: reference OCs. The young star clusters NGC 6611, NGC 6823, Bochum 1, NGC 2244 and NGC 2239 are indicated for comparison purposes. Analytical relations in panels (d) and (e) are discussed in the text. Dotted line in panel (c): Salpeter's IMF slope $\chi = 1.35$.

turnover at the subsolar mass range, as suggested by the IMFs of Kroupa (2001) and Chabrier (2003). However, given the low number of stars and the simplifying assumptions, we have omitted several possible systematic biases associated with the IMF determination: (i) uncertainties in the low-mass IMF due to differential reddening and possibly crowding (the latter should be minimal, since the objects are intrinsically poorly populated), (ii) missing companion stars (e.g. Maíz Apellániz 2008), (iii) binning (e.g. Maíz Apellániz 2005) and (iv) errors on the mass–luminosity relation of individual stars.

6 DISCUSSION

To put Pismis 5, vdB 80, NGC 1931 and BDSB 96 into perspective, their astrophysical parameters (Sections 3–5) are compared to those of a sample of nearby OCs in different environments. The reference sample contains some bright nearby OCs (Bonatto & Bica 2005; Bonatto et al. 2006b) together with a group of OCs projected towards the central parts of the Galaxy (Bonatto & Bica 2007a). The young OCs NGC 6611 (Bonatto et al. 2006c), NGC 6823 (Bica et al. 2008a) and NGC 2239 (Bonatto & Bica 2009b) are included for comparison with gravitationally bound objects of similar ages, while Bochum 1 (Bica et al. 2008a) and NGC 2244 (Bonatto & Bica 2009b) might be dynamically evolving into OB associations. All objects have been similarly analysed.

We work with the diagnostic diagrams shown in Fig. 12. Panels (a) and (b) examine the dependence of cluster ($R_{\rm RDP}$) and core ($R_{\rm c}$) radii on age, respectively. Pismis 5, vdB 80 and BDSB 96 (and to a lesser degree NGC 1931) present small $R_{\rm c}$ and $R_{\rm RDP}$, similar to NGC 6823 and typical of Gyr-old OCs undergoing disruption near the solar circle (e.g. Bergond, Leon & Guilbert 2001; Lamers

et al. 2005). Within uncertainties, the four objects follow the relation $R_{\rm RDP} = (8.9 \pm 0.3) \times R_{\rm C}^{(1.0\pm0.1)}$ (panel d), derived with the reference sample. They also appear to follow the relation of increasing OC size with Galactocentric distance[12] (panel f).

When the mass-density radial distribution follows a King-like profile (e.g. Bonatto & Bica 2007b,2008a; Bonatto et al. 2008), the mass inside $R_{\rm RDP}$ is a function of $R_{\rm c}$ and the central mass-surface density (σ_{M0}), $M_{\rm clus} = \pi\ R_C^2\ \sigma_{M0}\ \ln[1 + (R_{\rm RDP}/R_{\rm c})^2]$. With the relation between $R_{\rm c}$ and $R_{\rm RDP}$ (panel d), this equation becomes $M_{\rm clus} \approx 13.8\sigma_{M0}\ R_C^2$. The reference OCs, together with the present sample, are contained within King-like distributions with σ_{M0} constrained within $30 \lesssim \sigma_{\rm M0}({\rm M}_\odot\ {\rm pc}^{-2}) \lesssim 600$ (panel e). The exception is NGC 2244, which appears to present too big a core for the total mass.

Finally, when the total (MS+PMS) MF slope is considered (panel c), Pismis 5, vdB 80 and NGC 1931 present MFs significantly flatter than those of similarly young OCs. To a lesser degree, the same applies to the newly formed BDSB 96. Such flat slopes are equivalent to those derived for some very old OCs in the reference sample that, in general, undergo advanced dynamical evolution (e.g. Bonatto & Bica 2005). Given the young age, low mass, irregular RDP and the flat MF, the OCs NGC 1931 and Pismis 5 may be evolving into OB associations or remnants in a few 10^7 yr. Since both OCs are young, such effects may be related to another mechanism than age-related dynamical evolution. It is probably associated with star formation. vdB 80 and BDSB 96, on the other hand, appear to be typical young and low-mass OCs.

7 SUMMARY AND CONCLUSIONS

Probably because of the interplay between environmental conditions, star-formation efficiency and stellar mass, only a few per cent of the embedded clusters survive the first few tens of Myr. Thus, the derivation of astrophysical parameters of OCs in this phase may shed some light on the roles played by the above process in the dissolution/survival issue. In this context, poorly populated and massive OCs in different environments are yet to be investigated.

In the present paper, we derive astrophysical parameters and investigate the nature of the young and low-mass OCs Pismis 5, vdB 80, NGC 1931 and BDSB 96. The wide-field and near-infrared depth provided by 2MASS (with errors lower than 0.1 mag) are employed coupled to field-star decontaminated photometry. This enhances cluster CMD evolutionary sequences and stellar RDPs, yielding more constrained fundamental and structural parameters. The OCs are located within $174^\circ \lesssim \ell \lesssim 260^\circ$ and $|b| \lesssim 9^\circ$, thus, the errors potentially induced by the background star subtraction are not critical.

The decontaminated CMDs exhibit similar properties, basically a poorly populated MS, a dominant fraction of PMS stars together with some differential reddening. MS ages are constrained within 5 ± 4 Myr (Pismis 5, vdB 80, BDSB 96) and 10 ± 3 Myr (NGC 1931). However, the PMS stars suggest a wider age spread ($\sim$20 Myr), consistent with a non-instantaneous star formation process. The total (MS+PMS) stellar masses are low, within $\sim$60–180 $\rm M_\odot$, with MFs significantly flatter than Salpeter's IMF.

The present OCs are rather small ($R_{\rm c} \lesssim 0.48$ pc, $R_{\rm RDP} \lesssim 5.8$ pc), particularly Pismis 5 with $R_{\rm c} \approx 0.2$ pc and $R_{\rm RDP} \approx 1.8$ pc. Structurally, the (MS+PMS) stellar RDPs follow a cluster-like profile for most of the radius range. Exceptions are the inner regions of NGC 1931 and especially Pismis 5, which present a marked stellar-density excess. At $\sim$10 Myr, such a central cusp cannot result from large-scale cluster dynamical evolution. Instead, it probably is associated with molecular cloud fragmentation and/or star-formation effects.

BDSB 96 and vdB 80 present structural properties of typical young, low-mass OCs, although with flat MFs. On the other hand, the irregular RDPs – together with the low cluster mass and flat MFs – of NGC 1931 and especially Pismis 5 suggest that both OCs deviate from dynamical equilibrium. They are possibly evolving to become OB associations or remnants in a few 10^7 yr.

[12] It may be partly primordial, in the sense that the high molecular gas density in central Galactic regions may have produced small clusters (e.g. van den Bergh, Morbey & Pazder 1991).

ACKNOWLEDGMENTS

We thank the anonymous referee for interesting suggestions. We acknowledge support from the Brazilian Institution CNPq. This publication makes use of data products from the 2MASS, which is a joint project of the University of Massachusetts and the Infrared Processing and Analysis Centre/California Institute of Technology, funded by the National Aeronautics and Space Administration and the National Science Foundation. This research has made use of the WEBDA data base, operated at the Institute for Astronomy of the University of Vienna.

REFERENCES

Ahumada A. V., Clariá J. J., Bica E., Dutra C. M., Torres M. C., 2001, A&A, 377, 845
Bergond G., Leon S., Guilbert J., 2001, A&A, 377, 462
Bessel M. S., Brett J. M., 1988, PASP, 100, 1134
Bhatt B. C., Pandey A. K., Mahra H. S., Paliwal D. C., 1994, Bull. Astron. Soc. India, 22, 291
Bica E., Bonatto C., 2008, MNRAS, 384, 1733
Bica E., Dutra C. M., Soares J., Barbuy B., 2003, A&A, 404, 223
Bica E., Bonatto C., Barbuy B., Ortolani S., 2006, A&A, 450, 105
Bica E., Bonatto C., Dutra C., 2008a, A&A, 489, 1129
Bica E., Bonatto C., Camargo D., 2008b, MNRAS, 385, 349
Bonatto C., Bica E., 2003, A&A, 405, 525
Bonatto C., Bica E., 2005, A&A, 437, 483
Bonatto C., Bica E., 2006, A&A, 455, 931
Bonatto C., Bica E., 2007a, MNRAS, 377, 1301
Bonatto C., Bica E., 2007b, A&A, 473, 445
Bonatto C., Bica E., 2008a, A&A, 477, 829
Bonatto C., Bica E., 2008b, A&A, 485, 81
Bonatto C., Bica E., 2009a, MNRAS, 392, 483
Bonatto C., Bica E., 2009b, MNRAS, 394, 2127
Bonatto C., Bica E., Girardi L., 2004, A&A, 415, 571
Bonatto C., Bica E., Santos J. F. C. Jr, 2008, MNRAS, 386, 324
Bonatto C., Kerber L. O., Bica E., Santiago B. X., 2006a, A&A, 446, 121
Bonatto C., Bica E., Ortolani S., Barbuy B., 2006b, A&A, 453, 121
Bonatto C., Santos J. F. C. Jr, Bica E., 2006c, A&A, 445, 567
Cardelli J. A., Clayton G. C., Mathis J. S., 1989, ApJ, 345, 245
Chabrier G., 2003, PASP, 115, 763
Chen W. P., Chen C. W., Shu C. G., 2004, AJ, 128, 2306
Dutra C. M., Santiago B. X., Bica E., 2002, A&A, 383, 219
Friel E. D., 1995, ARA&A 1995, 33, 381
Ghez A. M. et al., 2008, ApJ, 689, 1044
Girardi L., Bertelli G., Bressan A., Chiosi C., Groenewegen M. A. T., Marigo P., Salasnich B., Weiss A., 2002, A&A, 391, 195
Goodwin S. P., Bastian N., 2006, MNRAS, 373, 752
King I., 1962, AJ, 67, 471
Kroupa P., 2001, MNRAS, 322, 231
Lada C. J., Lada E. A., 2003, ARA&A, 41, 57

Lamers H. J. G. L. M., Gieles M., Bastian N., Baumgardt H., Kharchenko N. V., Portegies Zwart S., 2005, A&A, 441, 117
Lata S., Pandey A. K., Sagar R., Mohan V., 2002, A&A, 388, 158
Maíz Apellániz J., 2005, ApJ, 629, 873
Maíz Apellániz J., 2008, ApJ, 677, 1278
Massey P., Johnson K. E., De Gioia-Eastwood K., 1995, ApJ, 454, 151
Moffat A. F. J., Fitzgerald M., Jackson P. D., 1979, A&ASS, 38, 197
Naylor T., Jeffries R. D., 2006, MNRAS, 373, 1251
Pandey A. K., Mahra H. S., 1986, Ap&SS, 120, 107
Piskunov A. E., Schilbach E., Kharchenko N. V., Röser S., Scholz R.-D., 2007, A&A, 468, 151
Pismis P., 1959, Bol. Obs. Tonantzintla Tacubaya, 2, 37
Salpeter E., 1955, ApJ, 121, 161
Siess L., Dufour E., Forestini M., 2000, A&A, 358, 593
Skrutskie M. et al., 1997, in Garzon F. et al., eds, The Impact of Large Scale Near-IR Sky Surveys. Kluwer, Dordrecht, p. 187
Trager S. C., King I. R., Djorgovski S., 1995, AJ, 109, 218
Trippe S. et al., 2008, A&A, 492, 419
van den Bergh S., 1966, AJ, 71, 990
van den Bergh S., Morbey C., Pazder J., 1991, ApJ, 375, 594
Vogt N., Moffat A. F. J., 1973, A&AS, 9, 97

This paper has been typeset from a TEX/LATEX file prepared by the author.